

Compression Behavior of Low-Pressure Cast AMC Syntactic Foams with High Porosity



Pierre Kubelka, Alexander Martin Matz and Norbert Jost

Abstract This work presents a method for the manufacturing of closed-cell aluminum matrix composite syntactic foams (AMCSFs) using a modified and simplified low-pressure infiltration setup. The influence of different wrought and cast alloys on the compressive behavior of these foams was investigated. Through the use of a variety of different cast and wrought alloys, it was possible to determine the Al matrix' influence on the compressive behavior. The investigated AlX-Al₂O₃ syntactic foams were manufactured using hollow alumina spheres with AA1050, AA2024, AA5019, AA7075, and A356 Al alloys in the as-cast state. The results of the manufacturing process and the selected process parameters show a good dispersion of the spheres within the AlX matrix with a typical near randomly close-packed structure at the same time. The high-strength Al alloys AA2024 and AA7075 lead to a very brittle deformation behavior of the foams in the compression tests, with a strongly oscillating behavior plateau and relatively low plateau stress level. In contrast, the low- and mid-strength alloys AA1050, AA5019, and A356 show a more ductile behavior with less oscillation at a higher plateau stress level. By the five different combinations of the material partners, it was possible to make a statement about the ductility–strength relation of metallic syntactic foams in dependence on the base matrix.

Keywords Syntactic foams · Compressive behavior · Alumina spheres · Aluminum alloys · Casting

Introduction

Aluminum foams have been undergoing a fast-paced development in the last decades regarding their mechanical properties related to lightweight design. Due to the combination of aluminum as the base material with a porous structure, it is possible to provide a structure with multifunctional properties such as a high specific strength,

P. Kubelka (✉) · A. M. Matz · N. Jost
Institute for Materials and Material Technologies (IMMT), Pforzheim University, Tiefenbronner Straße 65, 75175 Pforzheim, Germany
e-mail: pierre.kubelka@hs-pforzheim.de

© The Minerals, Metals & Materials Society 2020
N. Dukhan (ed.), *Proceedings of the 11th International Conference on Porous Metals and Metallic Foams (MetFoam 2019)*, The Minerals, Metals & Materials Series, https://doi.org/10.1007/978-3-030-42798-6_11

good energy-absorbing capabilities, and a good damping behavior [1–3]. In this field, aluminum matrix composite syntactic foams (AMCSFs) have been regaining a lot of interest recently, owing to the possibility of cheaper production and materials. These closed-cell foam structures combine the two different aspects of minimizing the material's density as a foam with a simultaneous reinforcement of the Al-base material by the use of porous and hollow discontinuous reinforcements, respectively. However, this makes them a more suitable lightweight material in comparison to non-reinforced open- and closed-cell aluminum foams.

A wide range of different material combinations and structural effects of AMCSFs have been studied regarding their manufacturing and compressive properties. The investigated Al-base materials are ranging from pure Al [4–10], AlCu alloys [7, 11], AlMg alloys [7–9, 12], AlSi alloys [5–7, 13–19] up to AlZn alloys [7, 10]. The spherical reinforcements are typically represented by ceramics like alumina [6, 7, 9, 11], silicon carbide [18], perlite [17], glasses [8, 13], and mixtures of silica and alumina with other additives [4, 5, 7, 10, 12, 14–16, 19, 20] where the geometric parameters of the spheres can range from several microns up to several millimeters. Since these previous investigations were only covering individual Al-base and reinforcement matrix combinations, a comprehensive statement about the impact of the Al-base matrix on the compressive behavior of the AMCSFs cannot be given.

This study follows the approach of generating a holistic understanding of the impact of the Al-base matrix on the compressive behavior of AMCSFs with hollow alumina spheres. For this, mm-sized hollow alumina spheres combined with different commercial Al wrought alloys (AA1050, AA2024, AA5019, AA7075) and one cast alloy (A356) are being investigated. Together with a simplified and modified low-pressure infiltration casting method, it is possible to provide AMCSFs with different Al-base matrices manufactured under simplified constant conditions with unchanged geometric parameters. Undergoing compressive testing, it is possible to provide information on the impact of the base material onto the general deformation behavior regarding the strength and ductility of the AMCSFs.

Experimental Methods

Raw Materials

The materials used to produce the AMCSFs are represented by hollow alumina spheres and different Al wrought and cast alloys. The hollow Al₂O₃ spheres (hollomet GmbH, Dresden, GER) were made of commercial C799 alumina and had a mean outer diameter of 3.83 mm with a shell thickness of 150 μm. The only investigated cast alloy is the commercially most used alloy A356 (AlSi7Mg0.3) with the ability to be artificially aged. The investigated Al wrought alloys can be divided into natural hard alloys and alloys with the possibility to be artificially and naturally aged. In terms of natural hard alloys, AA1050 (Al99.5) and AA5019 (AlMg5) were

Table 1 Chemical composition of the different Al wrought and cast alloys used for the investigations (in wt%)

Alloy	Si	Fe	Cu	Mg	Mn	Zn	Ti	Cr	Al	Rest
AA1050	0.214	0.353	0.006	0	0.004	0	0.015	0.011	99.344	0.052
AA2024	0.394	0.235	4.369	1.649	0.798	0.123	0.007	0.007	92.300	0.076
AA5019	0.418	0.298	0.029	5.156	0.210	0.018	0.096	0.096	93.688	0.075
AA7075	0.322	0.262	1.692	2.480	0.096	5.666	0.194	0.194	89.200	0.061
A356	7.330	0.110	0.003	0.360	0.001	0	0.110	0.001	91.938	0.146

investigated. For alloys with the ability of natural aging, AA2024 (AlCu4Mg1) and AA7075 (AlZn5.5MgCu) were studied. The composition of the investigated alloys was analyzed using spark emission spectroscopy and is shown in Table 1. Elementary components indicated with a value of zero did not reach the lower threshold value of the measuring range.

Manufacturing

The AMCSFs were manufactured using a modified and simplified low-pressure casting method. The complete setup of the process with the prepared mold is shown in Fig. 1. The alumina spheres were placed into a boron-nitride-coated stainless steel mold with a square cross section of $20 \times 20 \text{ mm}^2$ and were gently tapped in order to achieve a randomly close-packed structure [21]. To maintain the dense packaging and to prevent floating of the spheres while being infiltrated by the molten aluminum, an AISI304 grid with a mesh size of 2 mm was clamped right above the package. The mold with the package was then heated up to a temperature of 600 °C and given into the casting machine. The infiltration of the alumina sphere package was done using an Indutherm VC500 vacuum-casting machine. The modified process used can be divided into the three different steps of *melting*, *casting/infiltration*, and *cooling*.

1. The *melting* of the Al alloys was performed inductively in Ar atmosphere under atmospheric normal pressure at a temperature of 1,000 °C. After finishing the process of melting, the temperature was held for several further seconds to gain uniform distribution of the elements and temperature within the melt.
2. The *casting* and *infiltration* were performed as a sequence of these two steps. The *casting* was done by pouring the melt onto the package without using any further pressurization of the Ar atmosphere. This led to a complete coverage of the cross section of the sphere package, enabling an uniform infiltration. The *infiltration* itself was set in after a short delay of 0.3 s through the pressurization of the melt with 1.5 bar by the Ar atmosphere. The pressure was being held up for a minimum of 5 s to maintain the complete infiltration of the package until the solidification of the AlX matrix took place.

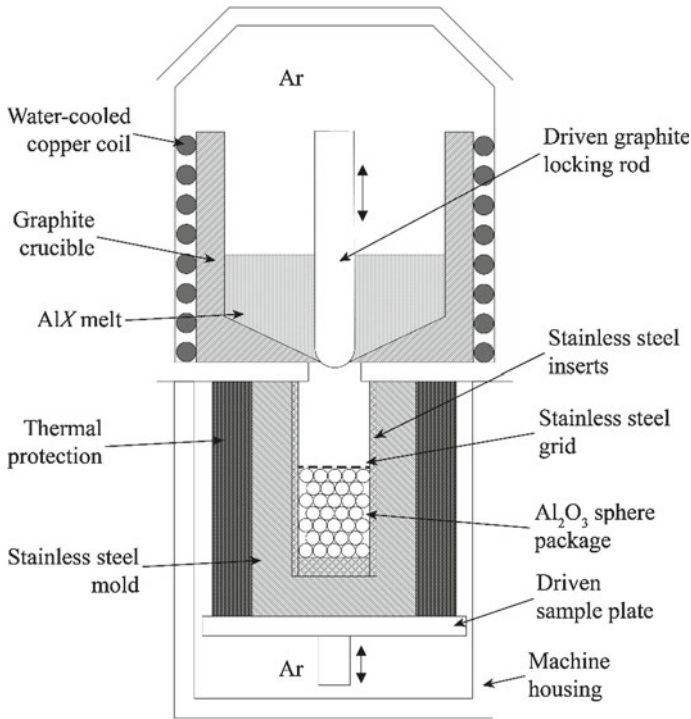


Fig. 1 Schematic setup of the modified and simplified low-pressure casting method within an Indutherm VC500 casting machine. The figure shows the process in the *melting* stage right before the *casting* and *infiltration*

3. The sample was cooled down within the machine and the mold to approximately 300 °C within 5 min. Afterward, the sample was demolded and cooled to RT in air.

The as-gained AlX-Al₂O₃ syntactic foam samples were finally machined to achieve defined geometric parameters. The foams were cut with a metal-bonded diamond cutting wheel in an ATM Brilliant 220 wet abrasive cutting machine to obtain samples with a length of 20 mm, which led to overall outer dimensions of 20 × 20 × 20 mm³. The separated surfaces of the samples were finally wet grinded with SiC abrasive paper to remove the remaining burrs and to smoothen the surface.

Compressive Testing

Prior to the compressive testing the relative densities ρ_{rel} of the samples for comparison purposes were calculated. For this, the outer dimensions and the weight of the samples were measured in order to calculate the density of the foams ρ_{foam} . This

Fig. 2 An example of the macrostructure of the as-cast AMCSFs



density was set in relation to the Al alloy's density ρ , resulting in the relative density of the foam (Eq. 1). With this procedure only the densities of the Al alloys were considered and the sphere's density was assumed to be identical. This small error could be neglected since identically produced samples were being compared in this investigation.

$$\rho_{\text{rel}} = \frac{\rho_{\text{foam}}}{\rho} \quad (1)$$

The compressive tests were performed using a Galdabini QUASAR 250 universal test rig. The compressive forces were applied onto the as-cast samples by using two hardened precision-grinded steel plates. The resulting deformation direction was perpendicular to the cut and ground sides and parallel to the casting direction. An example of the machined macrostructure of the as-cast AMCSFs is given in Fig. 2. At the beginning of the procedure, the samples were pre-compressed with a force F of 10 N. The testing was done using a displacement rate of 4 mm/min which corresponds to a strain rate of $3.33 \times 10^{-3} \text{ s}^{-1}$. The force–displacement data was recorded with a sampling rate of 100 s^{-1} to obtain the effective stress–strain curves for each individual sample until the maximum strain of 0.7. A force of 150 kN was set as the termination criterion for the tests.

Metallographic Analysis

To support the results of the deformation tests, the microstructures of AMCSFs were investigated. Therefore, slices perpendicular to the deformation direction were

machined and embedded in ClaroCit cold-mounting resin. The embedded specimens were ground and polished with diamond particles up to 1 μm . *Barker* etchant was used to develop the microstructure of the as-cast Al alloys. The optical characterization was performed using a Leica DMI5000M inverted light microscope.

Results and Discussion

Manufacturing and Microstructure

The low-pressure infiltration of the sphere package shows a relatively good sphere distribution with a nominal relative density of $\rho_{\text{rel}} \approx 56.5\%$, independent of the alloy investigated. The randomly close-packed structure, as a direct result of the tapping of the mold while placing the spheres and preventing the floating with a clamped stainless steel grid, remains almost unchanged in the as-cast samples. The microstructures of the different alloys have developed almost identically with a fine-grained and homogeneous microstructure within the samples (Fig. 3a, b). Only the AA5019 and AA7075 alloys are showing a gradation in the grain size from the inside to the outside. This is due to the lower solidification temperatures compared to the

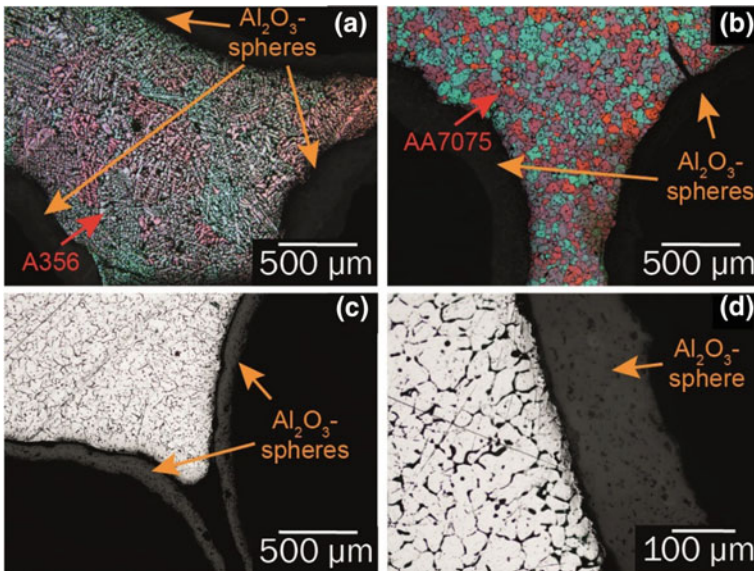


Fig. 3 Microstructures of different alloys as well as the filling and interfacial behavior between the constituents **a** microstructure of an as-cast A356 alloy, **b** microstructure of an as-cast AA7075 alloy, **c** infiltration behavior of the different Al alloys in spherical contact areas with voids, **d** interlocking between the solidified base matrix and the spherical reinforcement with small cavities

AA1050, AA2024, and A356 alloys. Looking at the micrographs of the ground and polished samples, an overall good interlocking between the AlX matrices and the alumina spheres can be detected (Fig. 3c, d). Small numbers of defects within the foam structures can also be noticed. In regions of interconnecting spheres, cavities with prematurely solidified melt fronts can be identified, which has also been reported by other researchers [17, 20]. Combined with small numbers of randomly distributed cavities at the interfaces, it follows that the used process parameters and pre-treatments of the materials do not yet correspond to the optimum for the production of cavity-free AMCSFs with this method. This problem can be solved by positively affecting the wetting behavior between AlX melt and the spheres in the infiltration stage. Due to the poor wetting of melted aluminum and its alloys with alumina, several changes can be made to minimize the contact angle between the two constituents. The change of the Al alloy composition under consideration of the Mg content as well as changes in the infiltration or mold temperatures can lead to better results [22, 23].

Compressive Behavior

Typical stress–strain curves for the different Al alloys investigated are shown in Fig. 4a. Compared to other investigations regarding melt infiltrated AMCSFs with mm-sized ceramic spheres [9, 17, 18, 20, 24, 25] an overall more brittle and oscillating behavior can be observed. This is due to the combination of the fast solidification of the melts while infiltrating the sphere package, the present microstructural conditions as well as the natural brittle behavior of the alumina spheres. Since only the influence of the Al alloys on the compressive behavior was investigated, the influence of the alumina spheres is not discussed below.

The melt solidifies within seconds and cools down to RT in less than 10 min, resulting in the fine-grained structure in the as-cast state. Residual stresses in the base matrix around the spheres occur during the rapid cooling because of the mismatch of the coefficients of thermal expansion of the AlX matrix to the alumina [26]. Comparing the five base materials with each other, a clear difference between the high-strength alloys (AA2024 and AA7075) and the low- to mid-strength alloys (AA1050, AA5019, and A356) can be observed. The high-strength alloys AA2024 and AA7075 can both be naturally and artificially aged [27, 28] resulting in a brittle matrix. Since the as-cast state provides relatively undefined microstructures, it must be assumed that partially artificial and natural aged conditions are present in the materials. The higher plastic collapse stresses σ_{pc} and the low plateau stresses σ_{pl} with a strongly oscillating plateau support this statement. The low- and mid-strength alloys AA1050, AA5019, and A356 are providing lower plastic collapse stresses with partially increased plateau stress levels (AA5019 and A356). These alloys have a much more ductile nature as the high-strength alloys as they are not able to be naturally aged. There are no finely dispersed sub-micron precipitations which inhibit a ductile behavior. Considering the maximization of the ductility with a simultaneous

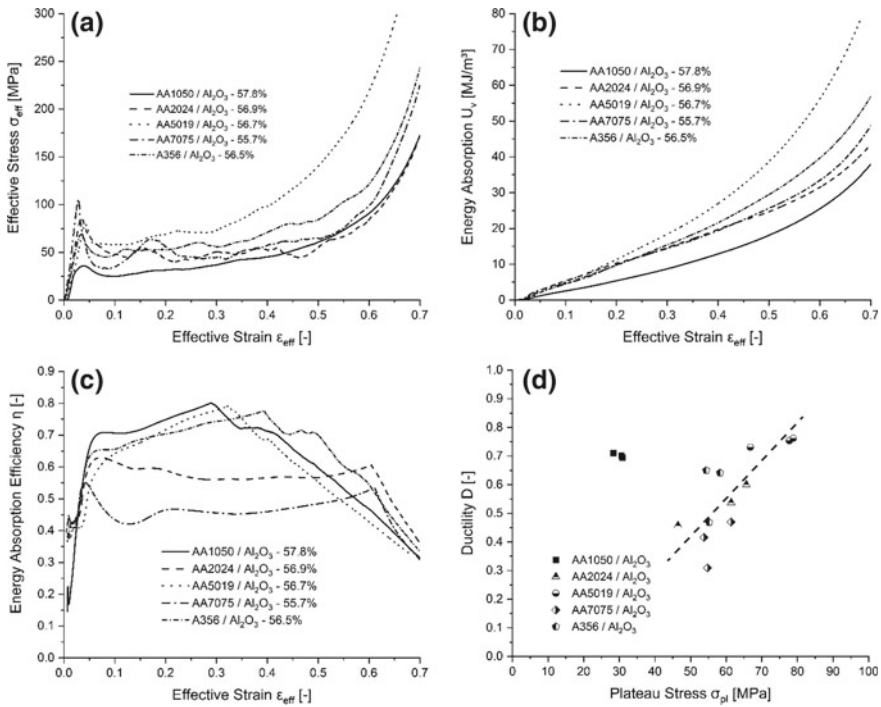


Fig. 4 **a** Effective stress–strain curves σ_{eff} (ϵ_{eff}) of all different AMCSFs investigated, **b** volumetric energy absorption curves $U_v(\epsilon_{eff})$ of all different AMCSFs investigated, **c** energy absorption efficiency curves $\eta(\epsilon_{eff})$ of all different AMCSFs investigated, **d** calculated ductility D versus the plateau stress σ_{pl} of all different AMCSFs investigated

high strength, the AA5019 alloy shows a pretty good behavior. This natural hard alloy cannot be artificially or naturally aged which is why a good ductility with a moderately high basic strength at the same time is maintained.

These different behaviors can also be verified by the energy-absorbing behavior. The energy absorption efficiency η shall be used for this assessment. It is defined as the actual absorbed energy under the stress–strain curve divided by the energy absorbed by an ideal absorber with the maximum stress σ_{max} reached up to the strain ϵ [29]. The energy absorption U_v [30] was calculated by Eq. 2 and the energy absorption efficiency was calculated by Eq. 3. The typical results of the energy absorption and efficiency for the different AMCSFs are displayed in Fig. 4b, c.

$$U_v = \int \sigma(\epsilon) d\epsilon \quad (2)$$

$$\eta = \frac{\int \sigma(\epsilon) d\epsilon}{\sigma_{max} \cdot \epsilon} \quad (3)$$

When considering the high-strength alloys AA2024 and AA7075, a pretty low overall efficiency can be observed. The massive stress drop from the plastic collapse stress down to a pretty low plateau stress level leads to a poor energy-absorbing performance. The buildup of narrow deformation bands with repetitive failure and rebuilding at higher strains leads to numerous small material breakouts within the foam until the densification of the foams. A very weak load distribution over all spheres onto the whole cross-sectional area of the foam is the result. Evaluating the energy absorption efficiencies of the three low- and mid-strength alloys, a higher overall efficiency can be observed. Their stress drops down to the plateau stress levels are smaller, positively affecting the energy absorption efficiency. These alloys are more ductile allowing a better load distribution within the matrix onto a higher number of ceramic spheres. Locally higher strains can be better cushioned which results in a much smoother plateau phase with less oscillation and break-ins. To make the influence of the AlX matrix on the ductility of the investigated AMCSFs tangible, a method for calculating such has been developed. This method describes the ductility D of these structures as the quotient of the minimum stress σ_{min} in the plateau phase (II) and the plastic collapse stress σ_{pc} (see Eq. 4). The plastic collapse stress is defined as the peak stress at which AMCSF transitions from the pseudo-elastic phase (I) to the plateau phase (II). Figure 5 displays the used parameters within the different phases summarized in a schematic plot.

$$D = \frac{\sigma_{min}}{\sigma_{pc}} \tag{4}$$

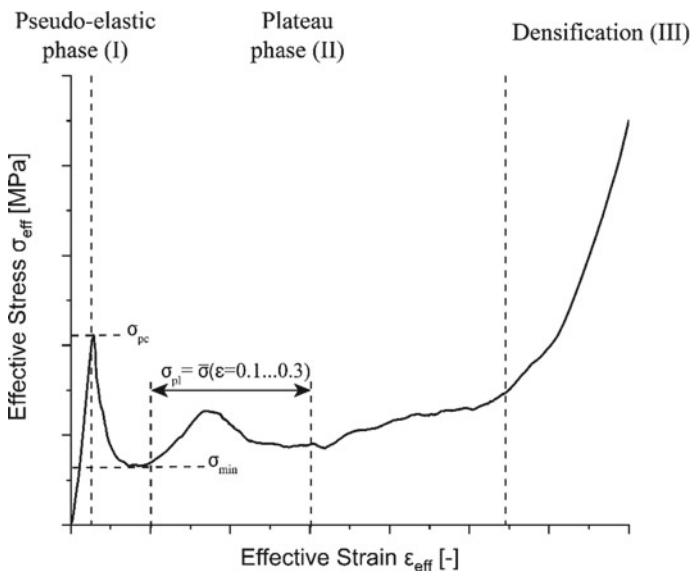


Fig. 5 Schematic plot of a brittle AMCSF showing the different compressive phases and the parameters used for the assessment of the overall ductility–strength behavior

Plotting the calculated ductility D above the plateau stress (mean stress between the strain of 0.1 and 0.3) of each individual investigated AMCSF sample results in a cloud of points which shows a linear relation between the ductility and strength of the foams as a function of the Al alloy (see Fig. 4d). Thereby, it can be shown that the selected base material and its condition have a substantial influence on the compressive deformation behavior and the strength of these structures. Multiphase high-strength AlX matrices (AA2024, AA7075) are negatively affecting the deformation behavior, while low- (AA1050) to mid-strength (AA5019, A356) alloys, with single- or dual-phase matrices, are positively affecting the ductility. The single-phase AA1050 (nearly pure Al) ensures that even softening with a simultaneous high ductility of the deformation behavior can occur. Multi-component alloys are therefore indispensable to achieve an increased overall strength of AMCSFs.

Conclusion

A modified and simplified low-pressure casting method was used to manufacture AMCSF samples with different AlX matrices to determine the impact of the base material on their compressive behavior. The produced samples were showing a near randomly dense-packed structure of the alumina spheres with small defects in the material's matrix (cavities and voids). The compressive tests have shown that the base materials have a significant influence on the deformation behavior of the AMCSF itself. High-strength alloys (AA2024, AA7075) have, in view of the as-cast states with an undefined phase composition, a negative impact onto the ductility and strength of the foams. Localized high strains ensure that an oscillating deformation behavior with a low plateau stress is achieved. Low- (AA1050) to mid-strength alloys (AA5019, A356) are more ductile, regarding the deformation behavior of the foam, because they are not as strongly affected by aging effects as the high-strength alloys. In comparison, it is possible to maximize the ductility and strength with these materials in the as-cast state. The developed method to calculate the ductility and plotting it above the plateau stress has demonstrated that not only the base material itself has an impact on the deformation behavior, but also the microstructural condition in which it is (as-cast, aged, ...) and the elemental composition of the alloys.

Acknowledgements The authors gratefully acknowledge financial support by the Europäischer Fonds für regionale Entwicklung (EFRE) and the Ministerium für Wissenschaft, Forschung und Kunst Baden-Württemberg within the research center ZAFH InSeL and the financial support through the program "Mittelbau" at HAW by the Ministerium für Wissenschaft, Forschung und Kunst Baden-Württemberg.

References

1. Ashby MF et al (2000) Metal foams: a design guide. Butterworth Heinemann, Burlington
2. Gibson LJ, Ashby MF (1997) Cellular solids: structure and properties. Cambridge University Press, Cambridge
3. Banhart J (2013) Light-metal foams—history of innovation and technological challenges. *Adv Eng Mater* 15(3):82–111
4. Xia X et al (2014) Compressive properties of closed-cell aluminum foams with different contents of ceramic microspheres. *Mater Des* 56:353–358
5. Szlancsik A et al (2017) On the effective Young's modulus of metal matrix syntactic foams. *Mater Sci Tech* 33(18):2283–2289
6. Su M et al (2019) Compressive properties of aluminum matrix syntactic foams prepared by stir casting method. *Adv Eng Mater* 21:1900183
7. Orbulov IN, Májlinger K (2013) Description of the compressive response of metal matrix syntactic foams. *Mater Des* 49:1–3
8. Lin Y et al (2017) Microstructure and strength correlation of pure Al and Al-Mg syntactic foam composites subject to uniaxial compression. *Mat Sci Eng A* 696:236–247
9. Castro G et al (2013) Compression and low-velocity impact behavior of aluminum syntactic foam. *Mat Sci Eng A* 578:222–229
10. Balch DK et al (2005) Plasticity and damage in aluminum syntactic foams deformed under dynamic and quasi-static conditions. *Mat Sci Eng A* 391:408–417
11. Santa Maria JA et al (2013) Al-Al₂O₃ syntactic foams—part I: effect of matrix strength and hollow sphere size on the quasi-static properties of Al-A206/Al₂O₃ syntactic foams. *Mat Sci Eng A* 582:415–422
12. Palmer RA et al (2007) Pressure infiltrated syntactic foams—process development and mechanical properties. *Mat Sci Eng A* 464:85–92
13. Wright A, Kennedy A (2017) The processing and properties of syntactic Al foams containing low cost expanded glass particles. *Adv Eng Mater* 19(11):1600467
14. Orbulov IN (2013) Metal matrix syntactic foams produced by pressure infiltration—the effect of infiltration parameters. *Mat Sci Eng A* 583:11–19
15. Tao XF et al (2009) Al matrix syntactic foam fabricated with bimodal ceramic microspheres. *Mater Des* 30:2732–2736
16. Tao XF, Zhao YY (2012) Compressive failure of Al alloy matrix syntactic foams manufactured by melt infiltration. *Mat Sci Eng A* 549:228–232
17. Taherishargh M et al (2015) On the particle size effect in expanded perlite aluminium syntactic foam. *Mater Des* 66:294–303
18. Luong DD et al (2013) Development of high performance lightweight aluminum alloy/SiC hollow sphere syntactic foams and compressive characterization at quasi-static and high strain rates. *J Alloy Compd* 550:412–422
19. Birla S et al (2017) Effect of cenosphere content on the compressive deformation behaviour of aluminum-cenosphere hybrid foam. *Mat Sci Eng A* 685:213–226
20. Myers K et al (2015) Quasi-static and high strain rate response of aluminum matrix syntactic foams under compression. *Compos Part A* 79:82–91
21. Jaeger HM, Nagel SR (1992) Physics of the granular state. *Science* 255(5051):1523–1531
22. Ip SW et al (1993) Wetting behaviour of aluminium and aluminium alloys on Al₂O₃ and CaO. *J Mater Sci Lett* 12(21):1699–1702
23. Klintner AJ et al (2008) Wetting of pure aluminum and selected alloys on polycrystalline alumina and sapphire. *Mat Sci Eng A* 495:147–152
24. Orbulov IN et al (2019) Compressive characteristics of bimodal aluminium matrix syntactic foams. *Compos Part A* 124:105479
25. Katona B et al (2019) Compressive characteristics and low frequency damping of aluminium matrix syntactic foams. *Mat Sci Eng A* 739:140–148
26. Arsenault RJ, Shi N (1986) Dislocation generation due to differences between the coefficients of thermal expansion. *Mat Sci Eng* 81:175–187

27. Guinier P (1938) Structure of age-hardened Aluminium-Copper alloys. *Nature* 142(3595):569–570
28. Berg LK et al (2001) GP-zones in Al-Zn-Mg alloys and their role in artificial aging. *Acta Mater* 49(17):3443–3451
29. Baumeister J et al (1997) Aluminium foams for transport industry. *Mater Des* 18(4–6):217–220
30. Paul A, Ramamurty U (2000) Strain rate sensitivity of a closed-cell aluminum foam. *Mat Sci Eng A* 281(1–2):1–7